Structural Eng. / Earthquake Eng. Vol. 3. No. 1, 73 s-82 s. April 1986
Japan Society of Civil Engineers (Proc. of JSCE No. 368/ I -5)

MODEL STUDIES ON SCATTERING OF ELASTIC WAVES IN A HALF SPACE

By Yoshiji NIWA, Sohichi HIROSE** and Shoichi NAKATANI****

Model studies are carried out to investigate the scattering behavior of elastic waves in a half space. The scatterers examined are a semi-circular surface irregularity and a circular cavity embedded in a half space. The detected waves are simulated by the boundary integral equation (BIE) method. The results show that the observed waves are slightly different from the simulated waves due to the resonance of transducer. In spectral analyses, therefore, we employ the linear system theory to eliminate the effect of transducer. The obtained frequency spectra reproduce an essential feature of the analytical results computed by the BIE method, except for their absolute values.

1. INTRODUCTION

Scattering problems of elastic waves are the major subjects in many fields, such as ultrasonics, applied mechanics, seismology, earthquake enqineering, and so forth.

In the fields of ultrasonics and applied mechanics, considerable model studies were reported on the scattering of elastic waves by simple obstacles in materials and structures, mainly in relation with non-destructive testings. The early work on the determination of frequency spectra of broadband ultrasonic pulses scattered in materials was done by Gericke[1]. The time records and their spectra of scattered pulses by various simple cavities and inclusions were investigated in detail by Sachse[2], Pao & Sachse[3], and Tittmann et al.[4)~6)] in order to characterize such scatterers. Excellent reviews on scattering problems in non-destructive testings were done by Sachse & Golan[7] and Tittmann[8]. In the field of ultrasonics, usually, only the scattered waves from some defects, not including any reflected waves from outer boundaries of a specimen, are analyzed, and compared with analytical solutions of scattering problems in an infinite medium.

In the fields of seismology and earthquake engineering, as contrasted with the case of ultrasonics, scattering problems in a half space are necessary to be solved. Several authors conducted experiments on wave propagations in a half space to investigate the effect of irregular surfaces and interfaces on seismic motions. Topographic effects on ground motions were studied experimentally by Rogers et al[9]. and Brune[10], and geological effects of sedimentary basins were investigated by King & Brune[11]. Rogers & Kisslinger[12] and Ohtsu et al[13]. carried out model studies on wave propagations in a dipping layer. In these

* Member of JSCE, Dr. Eng., Professor, Department of Civil Engineering, Kyoto University (Sakyo-ku, Kyoto 606)
** Member of JSCE, M. Eng., Instructor, Department of Civil Engineering, Kyoto University
*** Member of JSCE, M. Eng., Public Works Research Institute, Ministry of Construction (Tsukuba-gun, Ibaraki 305)

works, the observed data were compared with theoretical results based on the analytic method[11], the ray theory[12),13)], and the boundary integral equation (BIE) method[13].

In the present paper, experimental studies on scattering of elastic waves due to a surface irregularity or a cavity in a half space are conducted. The time-amplitude records and their spectra are compared with the theoretical results obtained by the BIE method, which has been well developed for the analyses of wave propagations in a half space[14)15)].

2. EXPERIMENTAL METHODS

(1) Apparatus

A diagram of the experimental apparatus is shown in Fig. 1. Commercial piezoelectric transducer A (NF Circuit Block, Tokyo, Model 905 S) was attached to the specimen and an electric step pulse was charged to the transducer. The nominal resonance frequency of the transducer is 1 MHz, and its weight is 10.1 g. The rise time of the step pulse was less than 3 nano-sec and the voltage was approximately 30 V. Elastic waves produced by transducer A propagated within the specimen and were detected as the electric signals by another transducer B. Transducer B is of the same type as transducer A and of longitudinal directivity[16]. Therefore, physical quantities of elastic waves detected by transducer B are considered as normal components to a free surface. The received signals were amplified with 60 dB total gain and bandpassed from 10 KHz to 300 KHz through the pre-amplifier and discriminator, and then recorded onto the floppy disks of a micro-computer at 0.2 μs sampling period through the transient recorder (NF Circuit Block, WM-852).

(2) Specimens

As shown in Fig. 2, the specimen was made of PMMA (polymethylmethacrylate) plate of 0.5 cm thickness, which was bonded to a brass rod. The PMMA plates had either a surface irregularity or a cavity at the portion of the right-hand slope as shown in the figure. The right-hand slope corresponds to a free surface, and the surface irregularity and cavity are scatterers in a half space. The surface irregularity was a semi-circle with the radius 1 cm, while the cavity was a circle with the radius 1 cm, the center of which was located at the depth of 1.5 cm from the free surface.

The velocity of the longitudinal wave (P wave) in the brass rod was 3 530 m/s, while the velocities of the longitudinal wave (P wave) and transverse wave (SV wave) in the PMMA plate were 2 410 m/s and 1 410 m/s, respectively. These wave velocities were measured from preliminary tests. The transmitter (transducer A) was attached at the end of the rod, and the receiver (transducer B) was placed on the free surface of the PMMA plate. Since the velocity of propagating wave in the rod is faster than those in the PMMA plate propagating waves in the rod are refracted into the PMMA plate, then generate P and SV waves at each point on the interface between PMMA plate and rod. It results in the generation of the plane P and SV waves as shown in Fig. 2.

The plane waves generated were propagated in the PMMA plate, reflected at the right-hand slope and

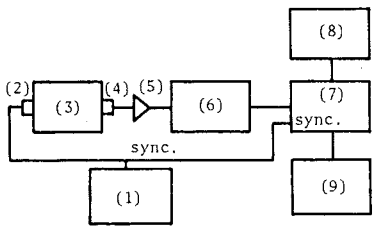

(1) Pulse generator
(2) Transducer A (transmitter)
(3) Specimen
(4) Transducer B (receiver)
(5) Pre-amplifier (20dB gain, 10kHz high-pass)
(6) Discriminator (40dB gain, 300kHz low-pass)
(7) Transient recorder
(8) Oscilloscope
(9) Microcomputer

Fig. 1 A block diagram of experimental setup.

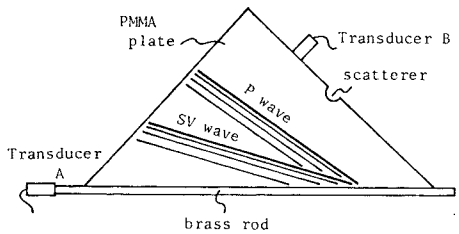

Fig. 2 A sketch of specimen.

scattered by the scatterers (surface irregularity and cavity), and then detected by transducer B.

The angle of the right-hand slope in Fig. 2 was changed in accordance with the incident angle of the plane P wave.

3. THEORY

In the spectral analyses discussed later, the frequencies in the range that $0.25<ak_L<4.0$ are taken into account, where a is the radius of scatterer and k_L is the wave number of the longitudinal wave in the PMMA plate. The wave length λ corresponding to these frequencies ranges from $1.55\ a$ to $24.1\ a$, which is much longer than the thickness $h(=0.5\ a)$ of the PMMA plate. Therefore, the displacement fields in the PMMA plate are reasonably assumed to be in a plane stress state. In this section, based on the above assumption, the formulations of BIE are presented briefly for scattering problems in a two-dimensional half space. Detailed formulations and numerical schemes are referred to Refs. 14) and 15).

(1) BIE formulation for a surface irregularity in a half space

Let D be a half space with a semi-circular surface irregularity ∂S, as shown in Fig. 3. The incident wave u^I is assumed to be a harmonic plane wave with the incident angle α. Then, the equation of motion and the boundary condition are written as below,

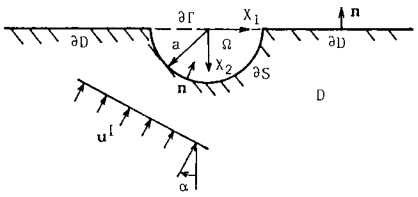

Fig. 3 Geometry of a surface irregularity in a half space.

equation of motion :

$$C_T^2\nabla^2 u(X,\omega)+(C_L^2-C_T^2)\nabla\nabla\cdot u(X,\omega)+\omega^2 u(X,\omega)=0 \quad X \text{ in } D \qquad (1)$$

boundary condition :

$$t(x,\omega)\equiv \overset{n}{T}u(x,\omega)\equiv\rho(C_L^2-2C_T^2)n\nabla\cdot u(x,\omega)+\rho C_T^2 n\cdot\{\nabla u(x,\omega)+(\nabla u(x,\omega))^T\}=0 \quad x \text{ on } \partial D \text{ and } \partial S \qquad (2)$$

where u, n, ω, ρ, C_T and C_L are the displacement vector, normal vector, angular frequency, mass density, and velocities of transverse wave and longitudinal wave in a plane stress state, respectively. Furthermore, the scattered field $u^S=u-(u^I+u^R)$ (u^R : the reflected field in the case of absence of the surface irregularity ∂S) satisfies the radiation condition[17] at infinity.

The problem is to find the solution $u(X,\omega)$ of Eq. (1), subjected to the boundary condition (2) and the radiation condition. In the case that the transient response $\hat{u}(X,t)$ is required, the inverse Fourier transform is available,

$$\hat{u}(X,t)=\frac{1}{2\pi}\int_{-\infty}^{\infty}u(X,\omega)e^{-i\omega t}d\omega. \qquad (3)$$

Taking account of the boundary condition (2), Green's formula leads to the following integral equation,

$$-\int_{\partial D}T(X,y)u^S(y,\omega)ds_y-\int_{\partial S}T(X,y)u(y,\omega)ds_y-\int_{\partial\Gamma}T(X,y)u^F(y,\omega)ds_y=\begin{cases}u^S(X,\omega) & X \text{ in } D \quad (4\cdot a)\\ -u^F(X,\omega) & X \text{ in } \Omega \quad (4\cdot b)\\ 0 & X \text{ in } D^C\cap\Omega^C \quad (4\cdot c)\end{cases}$$

where u^F is the free field defined as $u^F=u^I+u^R$. D^C is the complementary domain to the domain D, and $\partial\Gamma$ is the virtual boundary shown in Fig. 3. $T(X,y)$ is the double layer kernel defined as

$$T(X,y)=\overset{n}{T}_y U(X,y) \qquad (5)$$

where $U(X,y)$ is the fundamental solution of Eq. (1), which satisfies the radiation condition at infinity. $\overset{n}{T}_y$ is the traction operator as seen in Eq. (2). From the limiting process, X in $D^C\to x$ on ∂D or ∂S, the

boundary integral equations are obtained as follow,

$$-\int_{\partial D} T(x, y)u^S(y, \omega)ds_y-\int_{\partial S} T(x, y)u(y, \omega)ds_y$$
$$-\int_{\partial \Gamma} T(x, y)u^F(y, \omega)ds_y$$
$$=c^e u^S(x, \omega) \quad x \text{ on } \partial D \cdots\cdots (6\cdot a)$$
$$-\int_{\partial D} T(x, y)u^S(y, \omega)ds_y-\int_{\partial S} T(x, y)u(y, \omega)ds_y$$
$$-\int_{\partial \Gamma} T(x, y)u^F(y, \omega)ds_y+u^F(x, \omega)$$
$$=c^e u(x, \omega) \quad x \text{ on } \partial S \cdots\cdots (6\cdot b)$$

where $\int \cdot ds$ indicates the Cauchy's principal value integral, and $c^e u^S$ and $c^e u$ are the free terms of double layer potentials.

(2) BIE formulation for a cavity in a half space

For the model of a cavity in a half space as shown in Fig. 4, the equation of motion and the boundary condition are identical to Eqs. (1) and (2), respectively. Therefore, the following boundary integral equations for a cavity in a half space are obtained in the same form of Eq. (6),

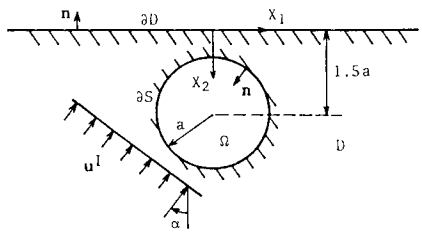

Fig. 4 Geometry of a cavity in a half space.

$$-\int_{\partial D} T(x, y)u^S(y, \omega)ds_y-\int_{\partial S} T(x, y)u(y, \omega)ds_y$$
$$=c^e u^S(x, \omega) \quad x \text{ on } \partial D \cdots\cdots (7\cdot a)$$
$$-\int_{\partial D} T(x, y)u^S(y, \omega)ds_y-\int_{\partial S} T(x, y)u(y, \omega)ds_y$$
$$+u^F(x, \omega)=c^e u(x, \omega) \quad x \text{ on } \partial S. \cdots\cdots (7\cdot b)$$

4. RESULTS AND DISCUSSION

(1) Amplitude-time records

Fig. 5 (a) shows the amplitude-time records observed at several points on the free surface in the case of semi-circular irregularity subjected to the vertical incidence of the primary longitudinal wave. Fig. 5 (b) is the case of semi-circular irregularity subjected to the oblique incidence ($\alpha=30^\circ$) of the primary wave. Fig. 5 (c) is the case of the cavity subjected to the oblique incidence ($\alpha=30^\circ$) of the primary wave. In these figures, the scale of amplitude is not absolute, because the characteristics of wave transmission from a specimen to a transducer and other equipments are unknown. Furthermore, the arrival time of initial wave motions is also relative, because it depends on the triggering of the transient recorder.

Fig. 6 shows the transient vertical displacements on the free surface synthesized by the BIE and inverse Fourier transform as discussed in the previous section. The models in Fig. 6 (a) to (c) correspond to those in Fig. 5 (a) to (c), respectively. In these transient analyses, we make the following remarks :

- The inverse Fourier transform (3) is carried out by using the fast Fourier transform (FFT) algorithm, where the frequencies up to $a(k_L)_{\max}\simeq 4$ are taken into account.
- The incident wave is the plane longitudinal wave, the pulse shape of which is assumed to be a Ricker wavelet

$$f(t)=2A'(\tau(t)-0.5)e^{-\tau(t)} (\tau(t)=(C_L k_L^P t)^2/4) \cdots\cdots (8)$$

where A' is the maximum amplitude of incident wave, and k_L^P is the peak wave number. We choose k_L^P as $(k_L)_{\max}/3$. The frequency spectra of a Ricker wavelet are limited in the narrow band, and are convenient for numerical calculations. This is why a Ricker wavelet is chosen as an incident signal.

- The maximum amplitude of a Ricker wavelet reaches the origin at the time $t=0$.

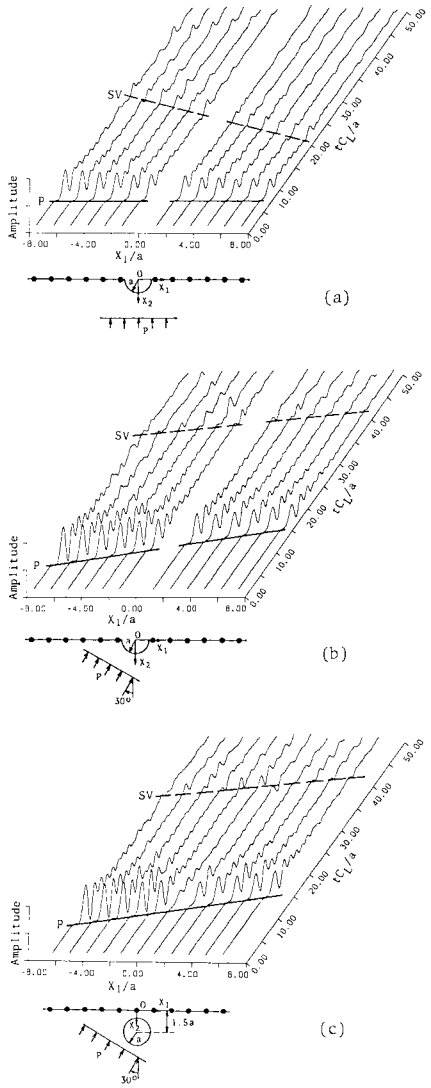

Fig. 5 Amplitude-time records observed on the free surface.

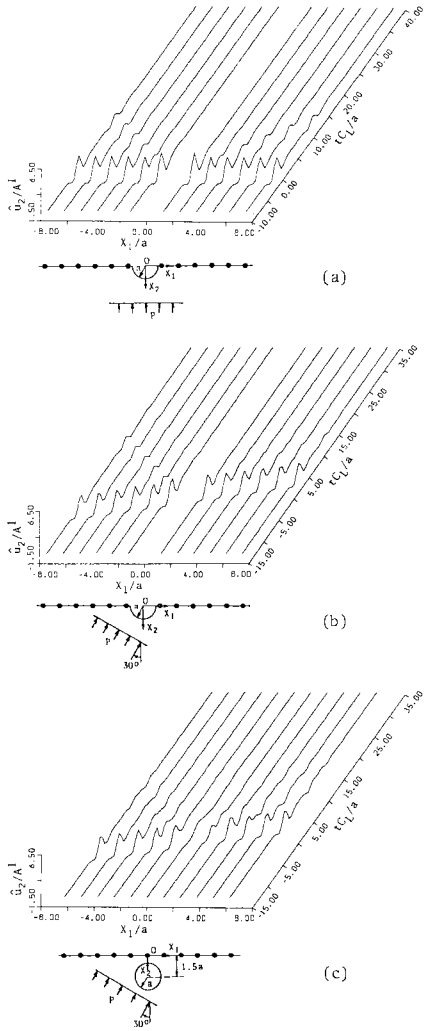

Fig. 6 Vertical components ($\hat{u}_2$) of transient surface displacements simulated by the BIE method. $\hat{u}_2$ is normalized by the maximum amplitude of a Ricker wavelet A'.

As above-mentioned, the characteristics of wave transmission from a specimen to a transducer, and vice versa, are unknown. Therefore, amplitudes and wave forms simulated with a Ricker wavelet as an incident wave do not necessarily coincide with those of observed data. However, the simulation analysis by the BIE is expected to provide a preliminary knowledge for the frequency analysis as shown later.

From comparisons between Fig. 5 and 6, it is concluded that

• In Fig. 6 (a) to (c), we can see two distinct travel-time curves. The one is related to the longitudinal incident wave. In the case of vertical incidence (Fig. 6 (a)), the incident wave reaches all observation points at the same time. In the cases of oblique incidence (Fig. 6 (b) and (c)), the incident wave arrives successively at the left-hand points to the right-hand points. The other travel-time curve is related to the scattered waves, which are generated by the scatterers and then propagated bilaterally along the free surface.

• As compared with Fig. 6, Fig. 5 shows more complicated features. There are a lot of tremors even

after the passage of the primary longitudinal wave. This phenomenon occurs due to the resonance of the transducers[16], which makes the scattered waves blurred.

• Apart from their waveforms, the travel-time curves with respect to the primary longitudinal wave and its scattered waves show a good agreement between the observed data and the theoretical results. In addition to these travel-time curves, Fig. 5 shows the secondary transverse wave, its scattered waves, the Rayleigh waves and reflected waves from the outer boundaries of the specimen, which are not taken into consideration in theoretical analyses.

(2) Frequency spectra

As seen in Fig. 5, the detected waves depend critically on the characteristics of transducers. In order to investigate spectral responses of elastic waves, therefore, the effect of transducer and other equipments must be removed. To this end, we analyzed detected waves on the basis of the linear system theory[7),16)].

If all components shown in Fig. 1 are considered as linear, the detected signal $o(t)$ and its Fourier transform $O(\omega)$ can be written as

$$o(t)=f(t)*w_m(t)*w_t(t)*w_u(t) \quad (9)$$

$$O(\omega)=F(\omega)\cdot W_m(\omega)\cdot W_t(\omega)\cdot W_u(\omega) \quad (10)$$

where $*$ denotes a convolution integral. $f(t)$ is the point force produced by transducer A. $w_m(t)$, $w_t(t)$ and $w_u(t)$ are the impulse response functions of specimen, transducer B and other apparatus, respectively. $F(\omega)$, $W_m(\omega)$, $W_t(\omega)$ and $W_u(\omega)$ correspond to Fourier transforms of $f(t)$, $w_m(t)$, $w_t(t)$ and $w_u(t)$, respectively.

In our experiments, another model specimen with the spectral response $W'_m(\omega)$ was employed. Detecting wave motions in these two models by use of the same monitoring system, we have the following relationship between $O(\omega)$ and $O'(\omega)$,

$$W_m(\omega)/W'_m(\omega)=O(\omega)/O'(\omega) \quad (11)$$

where $O'(\omega)$ indicates the Fourier transform of output signal of another model. We used the half space model without a surface irregularity or a cavity, as another model, whose spectral response $W'_m(\omega)$ was reasonably considered as flat. This leads to the conclusion that W_m/W'_m provides the spectral response of the model with the scatterer. Furthermore, W_m/W'_m does not include any effect of the transducer and other equipments. Thus, without specifying the characteristics of transducer and other equipments, we could determine the spectral response $W_m(\omega)/W'_m(\omega)$, and compared it with the theoretical result u_2/u_2^F.

In these spectral analyses, the data after the arrival of the secondary transverse wave were truncated. This procedure was consistent with the theoretical analyses for the incidence of longitudinal wave.

Fig. 7 shows the example of spectral amplitudes $|O(\omega)|$ and $|O'(\omega)|$ for the case of Fig. 8 (d). It is evident that $|O(\omega)|$ is quite different from the theoretical result, i. e., the solid line in Fig. 8 (d). This is because $O(\omega)$ involves the effect of transducer and other equipments which must be removed on the basis of Eq. (11). After applying the linear system theory to $O(\omega)$ and $O'(\omega)$, we can obtain reasonable spectral amplitudes as shown in the dashed line in Fig. 8 (d).

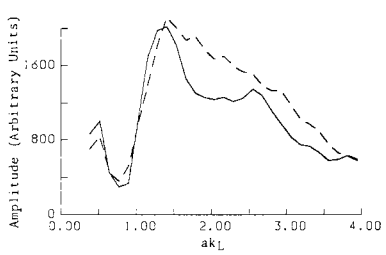

Fig. 7 Spectral amplitudes $|O(\omega)|$ (solid line) and $|O'(\omega)|$ (dashed line) for the case of Fig. 8 (d).

Fig. 8 illustrates the comparisons between the spectral amplitudes of vertical surface displacements ($|u_2/u_2^F|$) obtained experimentally and theoretically. This is the case of a half space with semi-circular surface irregularity for the vertical incidence of the longitudinal wave. Fig. 9 shows the case of the model with semi-circular surface irregularity for the oblique incidence (incident angle $\alpha = 30^\circ$) of the longitudinal wave. Fig. 10 shows the spectral amplitudes of surface displacements in the case that the longitudinal wave is obliquely incident ($\alpha=30^\circ$) on a cavity embedded in a half space. From these figures, the locations of the peaks and valleys in the

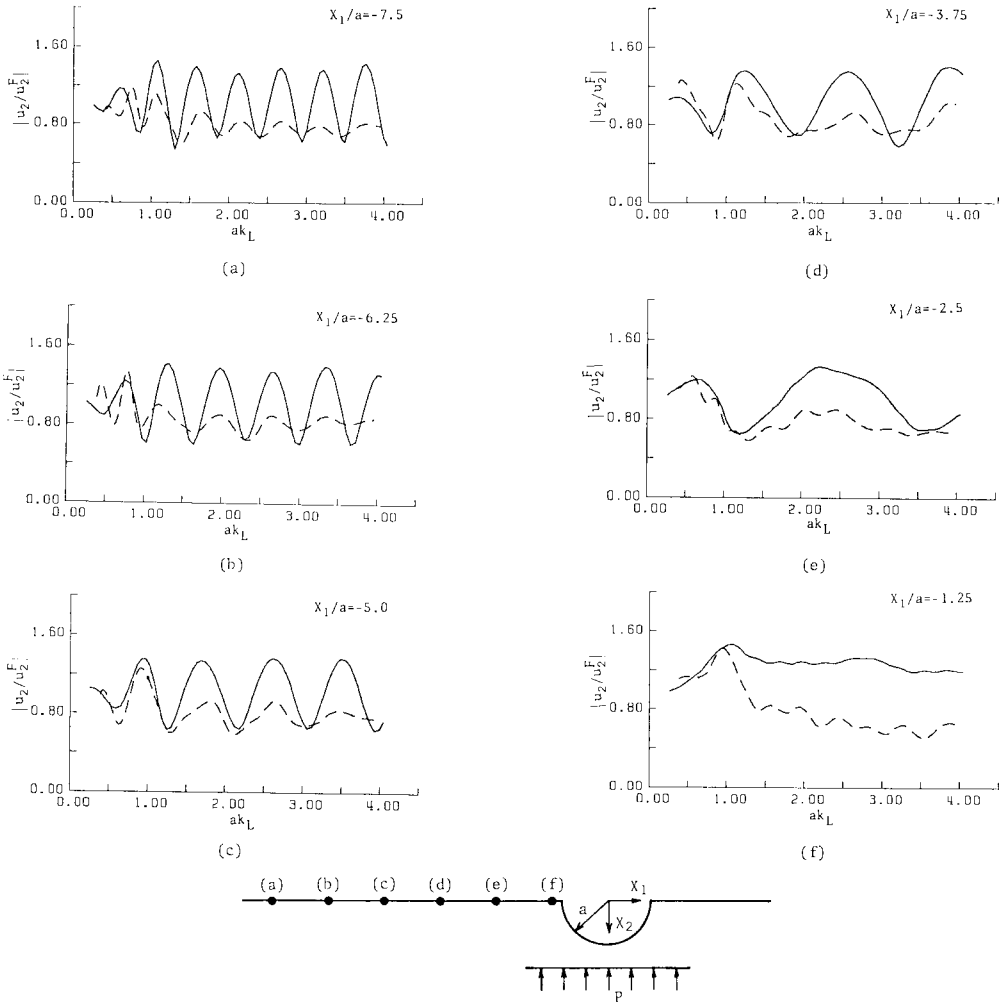

Fig. 8 Spectral amplitudes of vertical displacements (u_z) on the free surface. u_z is normalized by the vertical component of free field u_z^F. —— : BIE, ------ : experiment.

spectra obtained experimentally and theoretically agree well. The periodicity in the spectra at the point far from a scatterer can be understood in terms of the interference of the primary P wave and the scattered wave[7]. As for the absolute values of spectral amplitudes, however, a slight difference between experiment and theory is found. This may be caused for some reasons. First, the damping of specimens[18] diminishes the observed spectral amplitudes as compared with the calculated ones. In the high frequency range, especially, amplitudes at peaks and at troughs obtained from experiment attenuate more than those in BIE analysis. Furthermore, these phenomena are more remarkable as an observation point is remoter from a scatterer, since scattered waves propagate bilaterally from a scatterer. The second reason is an interaction between a transducer and a scatterer, particularly, at some points near a scatterer. Actually, large discrepancies between experiment and theory are found in Fig. 8 (f), 9 (f) and 10 (a):

5. CONCLUDING REMARKS

Model studies were carried out to investigate scattering of elastic waves in a half space. Experimental data were compared with theoretical results obtained by the BIE method. The amplitude-time records

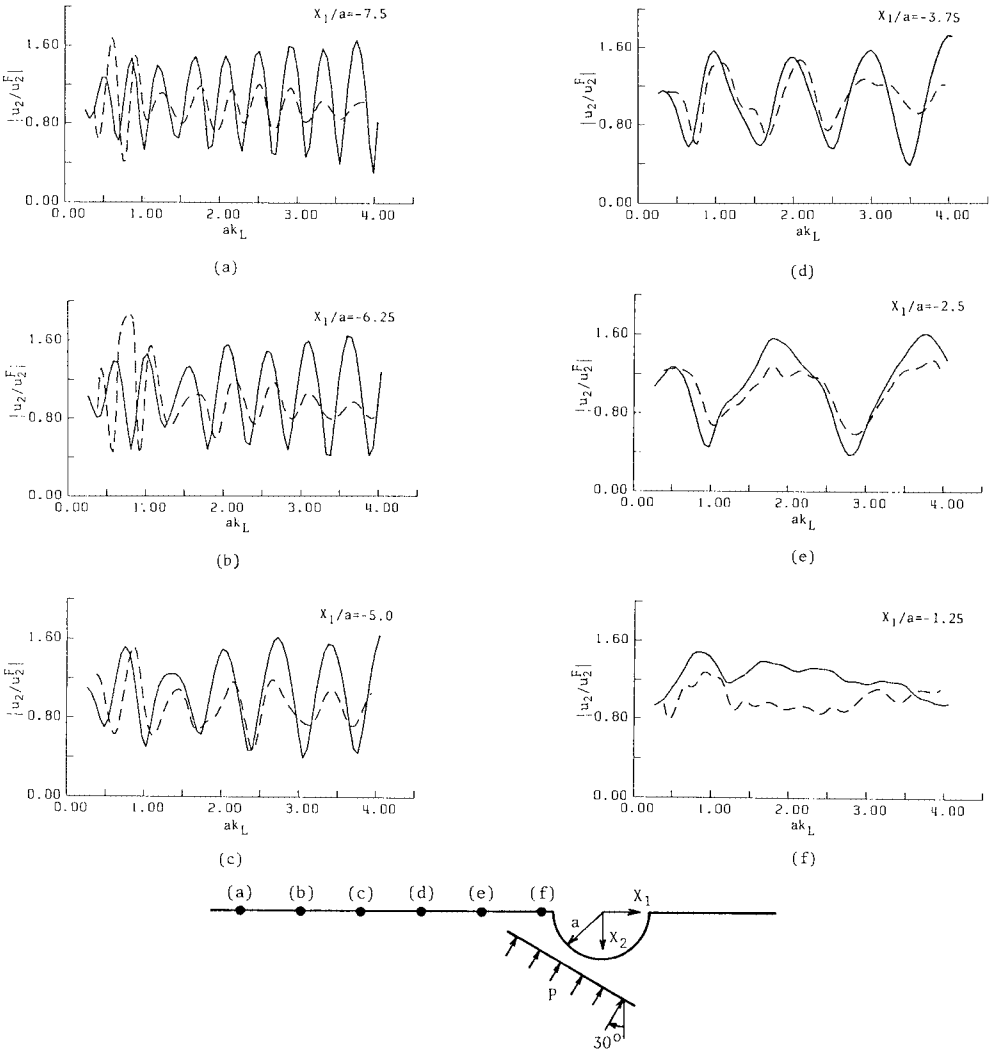

Fig. 9 Spectral amplitudes of vertical displacements (u_z) on the free surface. u_z is normalized by the vertical component of free field u_z^F. —— : BIE, ····· : experiment.

observed on a free surface were simulated by use of the BIE method and the FFT algorithm. Although the travel-time curves between experiment and theory showed a good agreement, the experimental scattered waveforms from a cavity or a surface irregularity were blurred due to the resonance of the transducer. In spectral analyses, we used the linear system theory in order to eliminate the effect of the transducer. While the obtained spectra reproduced an essential feature of theoretical results, it was found that the absolute values of spectral amplitudes had to be modified on account of the damping effect of specimens and the interaction between a transducer and a scatterer.

Here, only the simple models were analyzed. It is evident that the experimental method presented can be used to determine transient or spectral responses of complicated models, such as geological structures and testing members in ultrasonics.

ACKNOWLEDGMENT

The authors are indebted to Dr. M. Ohtsu who reviewed the manuscripts and made many helpful

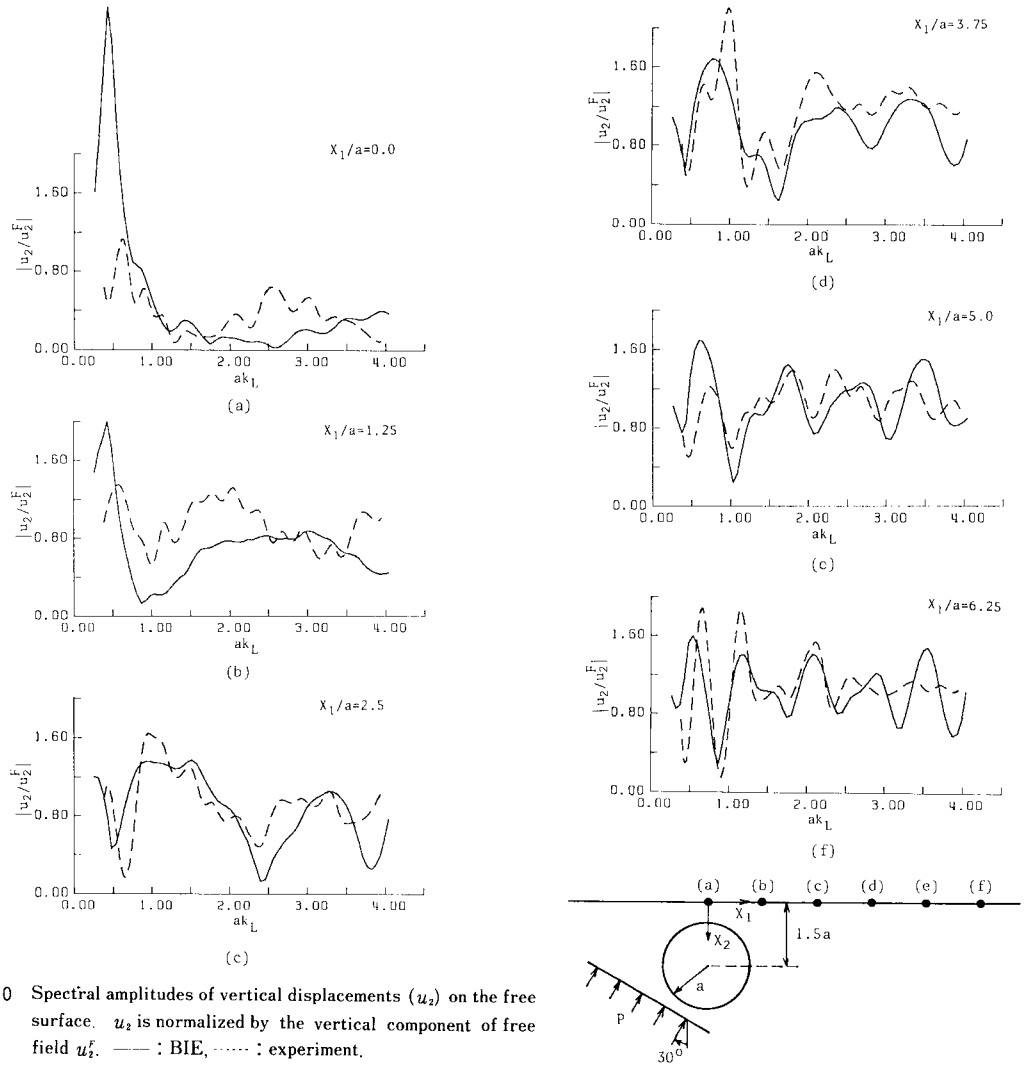

Fig. 10 Spectral amplitudes of vertical displacements (u_z) on the free surface. u_z is normalized by the vertical component of free field u_z^F. —— : BIE, ····· : experiment.

comments on them.

REFERENCES

1) Gericke, O. R. : Determination of the geometry of hidden defects by ultrasonic pulse analysis testing, J. Acoust. Soc. Am., Vol. 35, pp. 364~368, 1963.

2) Sachse, W. : Ultrasonic spectroscopy of a fluid-filled cavity in an elastic solid, J. Acoust. Soc. Am., Vol. 56, pp. 891~896, 1974.

3) Pao, Y.-H. and Sachse, W. : Interpretation of time records and power spectra of scattered ultrasonic pulses in solids, J. Acoust. Soc. Am., Vol. 56, pp. 1478~1486, 1974.

4) Tittmann, B. R., Cohen, E. R. and Richardson, J. M. : Scattering of longitudinal waves incident on a spherical cavity in a solid, J. Acoust. Soc. Am., Vol. 63, pp. 68~74, 1978.

5) Tittmann, B. R., Domany, E., Opsal, J. L. and Newman, K. E. : Elastic wave scattering from irregular voids, J. Appl. Phys., Vol. 54, pp. 6079~6085, 1983.

6) Tittmann, B. R. and Richardson, J. M. : Results on broadband scattering and diffraction suggest methods to classify and reconstruct defects in QNDE, New Procedures in Nondestructive Testing, editor : P. Höller, Springer-Verlag, pp. 277~285, 1983.

7) Sachse, W. and Golan, S. : The scattering of elastic pulses and the non-destructive evaluation of materials, Elastic Waves and

Non-Destructive Testing of Materials, editor : Y.-H. Pao, AMD-Vol. 29, pp. 11～31, 1978.

8) Tittmann, B. R : Scattering of elastic waves from simple defects in solids, A review, Wave Motion, Vol. 5, pp. 299～306, 1983.

9) Rogers, A. M., Katz, L. J. and Bennett, T. J. : Topographic effects on ground motion for incident P waves : A model study, Bull. Seism. Soc. Am., Vol. 64, pp. 437～456, 1974.

10) Brune, J. N. : Preliminary results on topographic seismic amplification effect on a foam rubber model of the topography near Pacoima dam, Proc. 8 th World Conf. Earthq. Eng., Vol. 2, pp. 663～670, 1984.

11) King, J. L. and Brune, J. N. : Modeling the seismic response of sedimentary basins, Bull. Seism. Soc. Am., Vol. 71, pp. 1469～1487, 1981.

12) Rogers, A. M. Jr. and Kisslinger, C. : The effect of a dipping layer on P-wave transmission, Bull. Seism. Soc. Am., Vol. 62, pp. 301～324, 1972.

13) Ohtsu, M., Hirose. S. and Niwa, Y. : Model studies on seismic ground motions in a dipping layer, Proc. 8 th World Conf. Earthq. Eng., Vol. 2, pp. 695～702, 1984.

14) Kobayashi, S. : Some problems of the boundary integral equation method in elastodynamics, Boundary Elements (Proc. 5 th Int. Conf.), Springer-Verlag, pp. 775～784, 1983.

15) Niwa, Y., Hirose, S. and Kitahara, M. : Application of boundary integral equation (BIE) method to transient response analysis of inclusions in a half space, Wave Motion, Vol. 8, pp. 77～91, 1986.

16) Niwa, Y., Kobayashi, S., Ohtsu. M. and Okuda, K. : Frequency spectra of acoustic emission, Proc. Japan Soc. Civil Eng., No. 314, pp. 137～147, 1981 (in Japanese).

17) Eringen, A. C. and Suhubi, E. S. : Elastodynamics, Vol. 2, Academic Press, 1975.

18) Niwa, Y. and Hirose, S. : Determination of acoustic emission source characteristics based on the moving dislocation theory, Progress in Acoustic Emisson II (Proc. 7 th Int. Acoustic Emission Symp.), Japan Soc. Non-Destructive Inspection, pp. 125～131, 1984.

(Received June 6 1985)